Influence of wall suction on the organized motion in a turbulent boundary layer

By R. A. ANTONIA†, L. FULACHIER‡,
L. V. KRISHNAMOORTHY†, T. BENABID‡
AND F. ANSELMET‡

† Department of Mechanical Engineering, University of Newcastle, NSW, 2308, Australia

‡ Institut de Mécanique Statistique de la Turbulence, Université d'Aix-Marseille,
13003 Marseille, France

The effect of wall suction on the organized motion of a tubulent boundary layer is examined experimentally both in a wind tunnel and in a water tunnel. In the wind-tunnel boundary layer, which developed over a slighly heated surface, temperature fluctuations were simultaneously obtained at several points, aligned in either the x (streamwise) or y (normal to the wall) direction. The temperature traces reveal the existence of two spatially coherent events, characterized either by a sudden decrease (cooling) or by a sudden increase (heating) of temperature. Estimates are presented for the average convection velocity, and average frequency of these events. The average convection velocity of 'coolings' is about 15 % larger than that of 'heatings', the velocity of both events exhibiting an important local maximum in the buffer region. Near the wall, the convection velocity of both events is increased slightly by suction while their average frequency is reduced by suction. Away from the wall, the average inclination of 'coolings' and 'heatings' is about 40° without suction; suction does not alter the inclination of 'coolings' but increases that of 'heatings' to about 50°. Visualizations in the water tunnel indicate that suction increases the stability and the longitudinal coherence of low-speed streaks. They also show that suction reduces the average frequency of dye ejections into the outer layer.

1. Introduction

The idea of treating turbulence as a black box is not new; in particular, the idea of perturbing a turbulent boundary layer (essentially a nonlinear system) and examining its response was suggested by Clauser (1956). Some of the information obtained by this approach has been reviewed by Tani (1969) and, more recently, by Smits & Wood (1985). The major conclusion that can be drawn from these reviews is that this information has provided very useful knowledge about the overall flow behaviour. However, the associated experiments were not aimed to investigate, at least directly, the response of the organized part of the flow to the perturbation. Such an aim seems important in the context of the recent interest in coherent structures. The present paper deals with a turbulent boundary layer which is subjected to a step change in surface suction. This choice was dictated primarily by the large amount of work that had previously been done on this type of change of surface condition at the Institut de Mécanique Statistique de la Turbulence (IMST) and elsewhere.

Previous, post-1965 studies (e.g. Favre *et al.* 1966; Aggarwal, Hollingsworth & Mayhew 1972; Fulachier 1972; Verollet 1972; Brosh & Winograd 1974; Eléna 1975,

1984; Fulachier, Verollet & Dekeyser 1977; Fulachier *et al.* 1982; Schildknecht, Miller & Meier 1979; Ramnefors & Nyden 1984) showed that for turbulent boundary layer and pipe flows the changes, when suction is applied, are mainly confined to the inner layer with a significant reduction in the intensity of velocity and temperature fluctuations. There was an accompanying reduction in the Reynolds shear stress and the lateral heat flux although the skin-friction coefficient and Stanton number increase owing to the additional momentum and thermal fluxes associated with the suction velocity (see e.g. Fulachier *et al.* 1982, 1987). Eléna (1975) and Fulachier *et al.* (1982) reported that the mean period of bursting was increased by suction and conjectured that suction should tend to make the viscous sublayer more orderly and therefore increase the anisotropy of the near-wall flow. It was also argued that suction diminishes the transverse motion more than the longitudinal motion.

The main aim of the present investigation is to focus, more directly than in previous studies, on the effect of suction on the organized motion in a turbulent boundary layer. The particular approach followed was to identify several features of this motion in a wind tunnel and in a water tunnel. In the wind tunnel, the main strategy was to introduce temperature as a passive marker of the flow and to use spatial arrays of cold wires for identifying events which were described by Chen & Blackwelder (1978) as internal temperature fronts or rapid coolings. A close examination of the present temperature traces also revealed the existence, previously reported by Subramanian *et al.* (1982), of spatially coherent events which are described here as heatings, since they are associated with a relatively sudden increase in temperature. Both 'coolings' and 'heatings' are studied and three of their characteristics – the average convection velocity, average frequency and average shape – have been determined. The focus on these events is justifiable in view of the possibility that they provide a dynamic link between near-wall and outer regions of the layer and of their possible association with the vortex loops or hairpin vortices observed by Head & Bandyopadhyay (1981). The flow visualizations were carried out in a water tunnel especially designed for this purpose. Despite the low Reynolds number in the water tunnel and the inherent limitations of visualization, the latter complemented, in an important way, quantitative information obtained in the wind tunnel where, in any case, the speed was too high to permit visualizations of reasonable quality. By introducing dye at the wall, we were able to visualize the effect of suction on low-speed wall streaks and on the trajectory of the dye as it moves into the outer layer.

2. Experimental arrangement and conditions

Figure 1 is a schematic representation of the experimental situation for which measurements and flow visualizations were made in the wind tunnel and water tunnel.

In the wind tunnel, the boundary layer developed on a horizontal 3.05 m long (0.56 m wide) smooth (impervious) metal surface followed by a 1.8 m long (0.56 m wide) porous surface. The impervious and porous walls were heated to a constant temperature T_w relative to the ambient temperature T_1 of 10 K. Over a longitudinal distance of about $\pm 5\delta$ (δ is the boundary-layer thickness) relative to the measurement station, T_w is constant (± 0.1 K).

The porous wall is made up of two alundum sections, of equal length and of 2 cm thickness. Detailed characteristics of this surface can be found in Verollet (1972) but it should be noted that the equivalent roughness height ϵ of this surface was
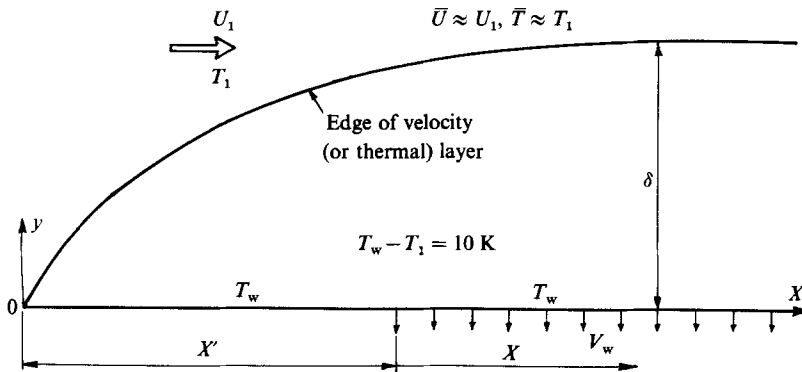
FIGURE 1. Definition sketch and schematic arrangement for wind-tunnel and water-tunnel (case H1) experiments.

estimated to be about 20 µm. The roughness Reynolds number ϵ^+ ($\equiv \epsilon U_\tau/\nu$; in general, the superscript $+$ will denote normalization by wall variables such as the friction velocity U_τ, the kinematic viscosity ν and the friction temperature $T_\tau = Q_w/U_\tau, Q_w$ being the thermometric wall heat flux) varied from 0.6 without suction to 0.9 with suction, suggesting that the surface is aerodynamically smooth in both cases.

The mass flux density through the porous wall is given by Darcy's law, viz.

$$\rho_w V_w = \frac{K}{\nu_w}\frac{\Delta p}{e},$$

where Δp is the pressure difference across the wall, e is the wall thickness, K is the coefficient of permeability of the wall material and V_w the velocity normal to the wall. When the wall temperature is increased, ν_w is also increased so that Δp must also be increased to maintain the same value of $\rho_w V_w$. For the present conditions, Δp was increased by 6% when the surface was heated. The estimated uncertainty in Δp ($\pm 0.5\%$) is smaller than that for the measured value of K ($\pm 3\%$). As a result of these uncertainties and because of the non-perfect homogeneity of the porous wall, the maximum variation in $\rho_w V_w$ over the full streamwise extent of the porous wall was $\pm 6\%$†.

Most of the measurements were made at a distance $X = 640$ mm from the start of the porous section. Without suction, δ was approximately 62 mm and the momentum-thickness Reynolds number R was 4900 (U_1 was nominally 12 m/s). The friction velocity $U_\tau = 0.48$ m/s ($c_f = 32 \times 10^{-4}$) and the friction temperature $T_\tau = 0.42$ K (Stanton number $St = 16.7 \times 10^{-4}$). For all measurements, with and without suction, temperature acted as a passive scalar: a typical value of the ratio Gr/Re^2 (where Gr is the Grashof number $g\delta^3(T_w - T_1)/\nu^2 T_1$ and Re is the Reynolds number $U_1\delta/\nu$) is 1.4×10^{-4} for the present conditions. The pressure gradient was slightly negative, the Clauser parameter $\pi = (\delta^*/\rho U_\tau^2)\,\mathrm{d}p_1/\mathrm{d}x$ being equal to -0.019 (the displacement thickness δ^* was 8.1 mm). The magnitude of the wall suction velocity V_w was $0.003U_1$ (or $A^+ = -\rho_w V_w/\rho_1 U_\tau = 0.055$). With suction at $X = 640$ mm, $\delta = 57$ mm, $U_\tau = 0.67$ m/s ($c_f = 62 \times 10^{-4}$), $T_\tau = 0.55$ K ($St = 31 \times 10^{-4}$). The magnitude of the pressure gradient ($\pi = 0.009$, with $\delta^* = 6.2$ mm) was slightly positive.

† Unless otherwise noted, uncertainties were estimated by the method of propagation of errors at 20:1 odds (Kline & McLintock 1953).

In the wind tunnel, the determination of U_τ was made by a number of different methods. For $A^+ = 0$, one determination used the Clauser-chart approach. The mean velocity profiles (measured with a Pitot tube connected to a MENSOR pressure transducer) were fitted to the log law

$$\bar{U}^+ = \kappa^{-1} \ln y^+ + C, \tag{1}$$

where $\kappa = 0.4$ and the additive constant $C = 5.24$. The value of U_τ ($= 0.48$ m/s, $\pm 3\%$) was in close agreement with estimates (0.48 m/s$\pm 5\%$) obtained by the momentum-integral method or by the Ludwig–Tillman formula. The Preston-tube method yielded a value of 0.46 m/s ($\pm 3\%$). For $A^+ = 0.055$, the mean velocity profiles were fitted to the modified log law (e.g. Stevenson 1963; Verollet, Fulachier & Dekeyser 1977)

$$\frac{2[1 - (1 - A^+ \bar{U}^+)^{\frac{1}{2}}]}{A^+} = \kappa^{-1} \ln y^+ + C. \tag{2}$$

This value of U_τ agreed to within $\pm 2\%$ of that determined by the momentum-integral method.

Mean temperature profiles were measured with a 1.2 μm cold wire, with a length of about 0.9 mm or 27 viscous units ($A^+ = 0$). In the form $(T_w - \bar{T})/(T_w - T_1)$, these profiles were identical with those obtained by Fulachier (1972) with a chromel–constantan thermocouple for $T_w - T_1 = 22$ K. Two methods were used to determine T_τ. One was based on the assumed temperature distribution in the sublayer, viz.

$$\Theta^+ = Pr\, y^+ \quad (A^+ = 0), \tag{3}$$

and

$$\Theta^+ = [1 - \exp(-A^+ y^+ Pr)]/A^+ \quad (A^+ = 0.055), \tag{4}$$

where $\Theta^+ = (T_w - \bar{T})/T_\tau$ and Pr is the molecular Prandtl number. This method yielded the following values of T_τ: 0.42 K ($\pm 3\%$) for $A^+ = 0$ and 0.55 K ($\pm 5\%$) for $A^+ = 0.055$. The corresponding Stanton numbers, $St = U_\tau T_\tau / U_1(T_w - T_1)$, were 16.7×10^{-4} ($A^+ = 0$) and 31×10^{-4} ($A^+ = 0.055$). For $A^+ = 0$, the Stanton number–Reynolds number relation given in Kays (1966) yielded 17×10^{-4} while the Prandtl–Taylor form of this relation, given in Brun, Martinot-Lagarde & Mathieu (1970), yielded 16.9×10^{-4}. Estimates of T_τ were also obtained by assuming logarithmic distributions, viz.

$$\Theta^+ = \kappa_\theta^{-1} \ln y^+ + C_\theta \quad (A^+ = 0), \tag{5}$$

$$\frac{2Pr_t[1 - (1 - A^+ \Theta^+)^{1/2Pr_t}]}{A^+} = \kappa_\theta^{-1} \ln y^+ + C_\theta \quad (A^+ = 0.055), \tag{6}$$

where $\kappa_\theta = \kappa/Pr_t$ (Pr_t is the turbulent Prandtl number assumed equal to 0.91) and $C_\theta = 3.1$. The resulting values of T_τ agreed to within $\pm 4\%$ with those inferred from (3) and (4).

Near-wall measurements of velocity fluctuations u (longitudinal direction) and w (spanwise direction) were made with a specially designed V-shaped probe (5 μm diameter hot wires). The complete length (1.6 mm between prongs) of the Wollaston (Pt–10% Rh) wires was etched. The wires were operated with DISA 55M10 constant-temperature circuits at an overheat ratio of 1.6. The wires were welded on four independent prongs, with an included angle of 65°. The wire centres are separated by a distance of 0.86 mm or 26 viscous units ($A^+ = 0$). In the near-wall region, where measurements were made (figure 2), the values of u' (the prime denotes an r.m.s. value) are nearly identical with those measured with a single hot wire; without
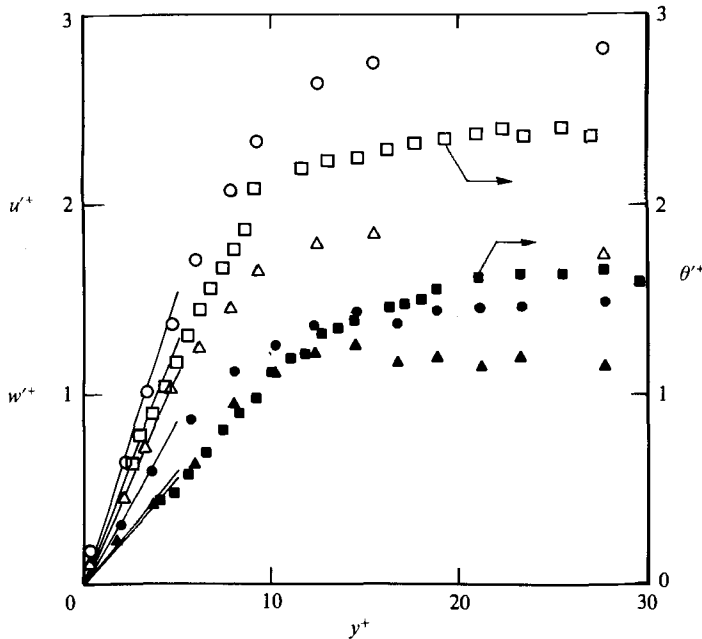
FIGURE 2. Near-wall distributions of r.m.s. longitudinal and spanwise velocity fluctuations and of r.m.s. temperature fluctuation. $\bigcirc$, u'^+; $\triangle$, w'^+; $\square$, θ'^+. Open and closed symbols are for $A^+ = 0$ and $A^+ = 0.055$ respectively.

suction, the results are in close agreement with those of Klebanoff (1955) and Kreplin & Eckelmann (1979a). For $A^+ = 0$, the values of w'^+ are systematically larger than those of Kreplin & Eckelmann (e.g. at $y^+ = 7$, the difference is 15%); the present value of w'^+ at $y^+ = 40$ (not shown in figure 2) is however in good agreement with the first measurement point of Klebanoff (1955).

Over the region $15 \lesssim y^+ \lesssim 100$, the correlation coefficient $\rho_{uw} = \overline{uw}/u'w'$ was essentially zero (± 0.01) for $A^+ = 0$ and equal to -0.07 (± 0.01) for $A^+ = 0.055$. For $y^+ < 15$, the scatter was larger but the average value of ρ_{uw} was -0.05 (± 0.05), both for $A^+ = 0$ and $A^+ = 0.055$, providing reasonable support for the claim of a two-dimensional mean flow.

The temperature fluctuation θ was measured with single 0.63 μm cold wires, with a length-to-diameter ratio l_{cw}/d_{cw} in the range 1000–1600 ($19 < l_{cw}^+ < 31$). There was no significant dependence of θ' on this ratio. No compensation was made for the thermal inertia of these wires since the cutoff frequencies (-3 dB) of the wires were always larger than the frequency at which the spectral contribution to the temperature variance became negligible. For $\overline{U} = 10$ ms^{-1}, the cutoff frequency of a 0.63 μm wire is about 5 kHz (e.g. Antonia, Brown & Chambers 1981). To study heatings and coolings, an array of 0.63 μm wires was used, each wire having an active length 0.8 mm (± 0.1 mm). The wires, which lie in the same plane, are parallel to each other and normal to the mean flow direction. A maximum of eight wires was used, with a nominal separation between wires of 0.9 mm or $1430d_{cw}$. This separation is well in excess of the longitudinal distance of $150d_{cw}$ for which Hishida & Nagano (1978) found no influence of the wake of an upstream cold wire on a downstream hot wire. The separation (4 mm) between prongs supporting individual wires was also sufficiently large to minimize the effect of upstream prongs on downstream wires.

The same array was used in either of two configurations, one with the wires aligned in the x-direction and the other with the wires aligned in the y-direction. All cold wires were made of Wollaston (Pt–10% Rh) and operated with in-house constant-current (0.1 mA) circuits with identical amplitude and phase characteristics. Velocity and temperature fluctuations were usually recorded on analogue FM tapes and later digitized for computer processing (HP1000 or VAX 780). In some cases, direct digitial recordings were made on the HP1000 computer.

The closed-circuit water tunnel was described by Dumas, Domptail & Daïen (1982). For the present investigation, a porous plate (25 cm long, 16 cm wide) was installed on one of the sidewalls of the 20 cm × 20 cm vertical working section (height ≈ 1.2 m) of the tunnel. Visualizations were made for two different configurations of the porous plate. In the first case (H1), which corresponds to the configuration depicted in figure 1, the leading edge of the plate was 64 cm downstream of the beginning of the working section where the boundary layer is fully developed. In the second case (H2), the wall containing the porous plate was turned upside down so that the boundary layer first developed on the porous plate, the visualizations being made of the boundary layer on the impervious surface downstream of the porous surface. This configuration, in which the boundary layer is subjected to a sudden removal of wall suction and is therefore in a state of relaxation, differs significantly from case H1 (figure 1). In both cases roughness was used to fix transition and to generate a relatively thick turbulent boundary layer. The roughness consisted of two strips, separated by 29 mm in the x-direction. Each strip was 28 mm wide and spanned the full width of the working section. For the upstream strip, pebbles of average diameter ≈ 4 mm and average height ≈ 5 mm were used. For the downstream strip, the average pebble diameter was 3 mm while the average height was 3 mm (maximum variation ± 1 mm). Mean velocity measurements were made only for the H1 configuration, using a laser-Doppler anemometer fitted with a Bragg cell. At $X = 100$ mm, the boundary-layer thickness δ was 50 mm ($U_1 = 16$ cm/s, $U_\tau = 0.78$ cm/s, $c_f = 47.7 \times 10^{-4}$) and the corresponding momentum-thickness Reynolds number R was 620. Four suction rates were used for H1: $A^+ = 0.014$ (with $V_w = -0.0007U_1$ and $U_\tau = 0.80$ cm/s), $A^+ = 0.026$ (with $V_w = -0.0014U_1$ and $U_\tau = 0.86$ cm/s), $A^+ = 0.047$ (with $V_w = -0.003U_1$ and $U_\tau = 0.95$ cm/s), $A^+ = 0.072$ (with $V_w = -0.0048U_1$ and $U_\tau = 1.07$ cm/s). For H2, only one rate of suction was used: $A^+ = 0.072$ with $V_w = -0.0048U_1$.

Without suction, the determination of U_τ in the water tunnel was made by fitting the measured velocity profiles to (1) with an accuracy of about $\pm 3\%$. For this value of U_τ, the velocity distribution in the part of the sublayer that was amenable to measurement ($y^+ \gtrsim 2.5$) followed the linear law $U^+ = y^+$ adequately ($\pm 8\%$). With suction, U_τ was obtained by fitting to (2), the sublayer data agreeing ($\pm 8\%$) with the relation $\bar{U}^+ = [1 - \exp(-A^+y^+)/A^+]$.

Dye was injected through:

(i) a 1 mm diameter hole on the wall centreline upstream of the roughness strip. This enabled the complete boundary layer to be marked with dye;

(ii) a 0.8 mm diameter hole on the wall centreline 63 mm upstream of the porous-plate leading edge (H1) or 63 mm downstream of the porous-plate trailing edge (H2). This enabled us to estimate the effect of suction on a single dye streakline that is introduced at the wall. The dye flow rate was 1.1 mm³/s corresponding to a wall injection velocity of $0.28U_\tau$;

(iii) a narrow slit (streamwise extent = 0.2 mm, spanwise extent = 180 mm) flush with the wall, 30 mm upstream of the porous plate for H1 or 30 mm downstream of

the porous plate for H2. This permitted the introduction, at the wall, of a thin sheet of dye. To avoid disturbing the near-wall flow, the dye flow rate was small (≈ 35 mm³/s); the corresponding wall injection velocity was about $0.12U_\tau$;

(iv) 0.8 mm diameter hypodermic tubes located in the three-dimensional contraction upstream of the working section, either for marking the edge of the boundary layer or for indicating the behaviour of individual dye streaklines within the boundary layer.

Two water-diluted dyes were used: fluorescein and rhodorsil (a white silicone oil emulsion). Photographs of the (x, y) (main shear) and (x, z) (spanwise)-planes, illuminated with narrow sheets of light, were taken using a synchronized flash. Films were also made with a Super 8 mm camera of views in either the (x, y)-plane or the (x, z)-plane for H1 and H2.

3. Near-wall turbulence measurements

As was established in the previous studies, the magnitudes, in the inner region, of the Reynolds shear stress $\overline{u^+v^+}$, the heat flux $\overline{v^+\theta^+}$ and the r.m.s. intensities u'^+, v'^+, θ'^+ are reduced by suction. Since the smallest value of y^+ for which X-probe measurements could be made in our case was 30 for $A^+ = 0$ and 44 for $A^+ = 0.055$, it was not possible to measure v in the near-wall region. This is the reason why it was important to establish the behaviour, in this region, not only of u'^+ and θ'^+, but also of w'^+ which, to our knowledge, had not been previously measured in a boundary layer for $A^+ \neq 0$. The resulting distributions, obtained with the V-probe, for $y^+ \lesssim 45$ (figure 2) show that while w'^+ is reduced by suction, the reduction in u'^+ is slightly larger. The reduction in the maximum value of u'^+ is about 48% compared with about 32% for w'^+. For the largest suction rate considered in the pipe-flow study of Schildknecht *et al.* (1979), the reduction in the maximum value of u'^+ was almost twice as large as that in w'^+ and about 2.5 times as large as that in v'^+ but, for this experiment, suction was applied for a very short streamwise distance. The present observations and those of Schildknecht *et al.* (1979) are at variance with the conjecture by Eléna (1975) and Fulachier *et al.* (1982) that w'^+ would be most affected by suction. This conjecture was based on the observation that, within the viscous sublayer in a fully developed pipe flow, large-amplitude temperature fluctuations were more affected by suction than large-amplitude fluctuations in the longitudinal velocity. It was argued that since temperature depends on all three components of the velocity vector (Fulachier 1972) and since v is significantly smaller than u or w in the near-wall region, suction affects w more than u.

The reduction in the maximum value of θ'^+ is smaller (about 20%) compared with that in u'^+. But in fact, within the viscous sublayer, we estimate, from the slopes of the lines drawn in figure 2 for $y^+ \lesssim 5$, that $du'^+/dy^+ \approx 0.30 \pm 5\%$ and $d\theta'^+/dy^+ = 0.26 \pm 5\%$ when $A^+ = 0$ whereas $du'^+/dy^+ \approx 0.17 \pm 5\%$ and $d\theta'^+/dy^+ = 0.11 \pm 5\%$ when suction is applied. Near the wall,

$$\left(\frac{du'^+}{dy^+}\right)_{A^+ \neq 0} = 0.57 \left(\frac{du'^+}{dy^+}\right)_{A^+ = 0}, \quad \left(\frac{d\theta'^+}{dy^+}\right)_{A^+ \neq 0} = 0.42 \left(\frac{d\theta'^+}{dy^+}\right)_{A^+ = 0}$$

demonstrating that du'^+/dy^+ is less reduced by suction than $d\theta'^+/dy^+$. The reduction in the near-wall value of dw'^+/dy^+ ($0.22 \pm 9\%$ for $A^+ = 0$ and $0.12 \pm 9\%$ for $A^+ = 0.055$) is identical with that observed for du'^+/dy^+. The value of 0.26 for $d\theta'^+/dy^+$ when $A^+ = 0$ is in close agreement with that obtained by Krishnamoorthy &

Antonia (1986) who found that $d\theta'^{+}/dy^{+}$ was unaffected by the length-to-diameter ratio of the cold wire when this ratio was in the range of about 600 to 1800. The present value of dw'^{+}/dy^{+} is significantly larger than the limiting values of $(dw'^{+}/dy^{+})_{y^{+}=0}$ reported by Sirkar & Hanratty (1970), Py (1973) and Kreplin & Eckelmann (1979a). It should be underlined however that the lines in figure 2 may not represent estimates of slopes at the wall since no data were taken at very small values of y^{+}. For example, a linear fit to the w'^{+} data (extending to $y^{+} \approx 5$) of Kreplin & Eckelmann (their figure 6) yields a value for dw'^{+}/dy^{+} of about 0.20; in contrast, Kreplin & Eckelmann obtained a value of 0.065 for $(dw'^{+}/dy^{+})_{y^{+}=0}$ using hot films flush-mounted at the wall. This suggests that there is not necessarily any inconsistency between the present measurements and those obtained in other investigations with wall heat/mass transfer methods.

Simultaneous measurements of u and θ were made with a pair of wires (one hot, one cold) parallel to the wall and normal to the mean flow. The wires were at nominally the same distance from the wall. The magnitude of the correlation coefficient between u and θ was about -0.8. The close similarity between u and θ is apparently maintained when suction is applied and the stabilizing influence of suction is felt more strongly on the longitudinal than on the spanwise velocity fluctuations.

It should be noted that the decrease, due to the suction, in the r.m.s. intensities of figure 2 is exaggerated as a result of the normalization by the friction velocity and the friction temperature. The increases, due to suction, in U_{τ} and T_{τ} are equal to about 40% and 30% respectively.

4. Characteristics of temperature fronts

Traces of temperature signals obtained with the array of cold wires aligned in either the x- or y-directions exhibit relatively sudden decreases in temperature which are detected by all wires. These decreases are identified in figure 3 (y-array) by downward-pointing arrows. Figure 3 also shows increases in temperature (identified by upward arrows) which, although generally less abrupt than the decreases in temperature, are nevertheless also detected by all wires. Chen & Blackwelder (1978) used the term 'internal temperature front' to designate the spatially coherent decrease in temperature. They also interpreted this front as an internal shear layer since the decrease in temperature is accompanied by concomitant changes in velocity; they observed that this shear layer, which was associated with the back (upstream part) of the bulges in the turbulent/non-turbulent interface at the outer edge of the boundary layer, maintains its identity into the fully turbulent region of the layer. It may be preferable to avoid using the term 'front' since it has been established that it usually occurs at the 'back' of a bulge. Here we describe spatially coherent regions characterized by a sudden decrease of temperature as 'coolings' and refer to regions associated with a temperature increase as 'heatings'. Subramanian *et al.* (1982) found that a cooling can be identified with a boundary between a region (downstream) where $u < 0$ and $v > 0$ and a region where $u > 0$ and $v < 0$ (upstream); for a heating, the velocity fluctuations downstream of the boundary satisfy $u > 0$, $v < 0$ while those in the upstream region satisfy $u < 0$ and $v > 0$. Subramanian *et al.* used the terms sweeps and ejections to describe the $(u > 0, v < 0)$ region and $(u < 0, v > 0)$ region respectively. It is however recognized that these terms, first introduced by Corino & Brodkey (1969), strictly describe the physical events characterized by the motion toward the wall of relatively high-speed fluid (sweep)
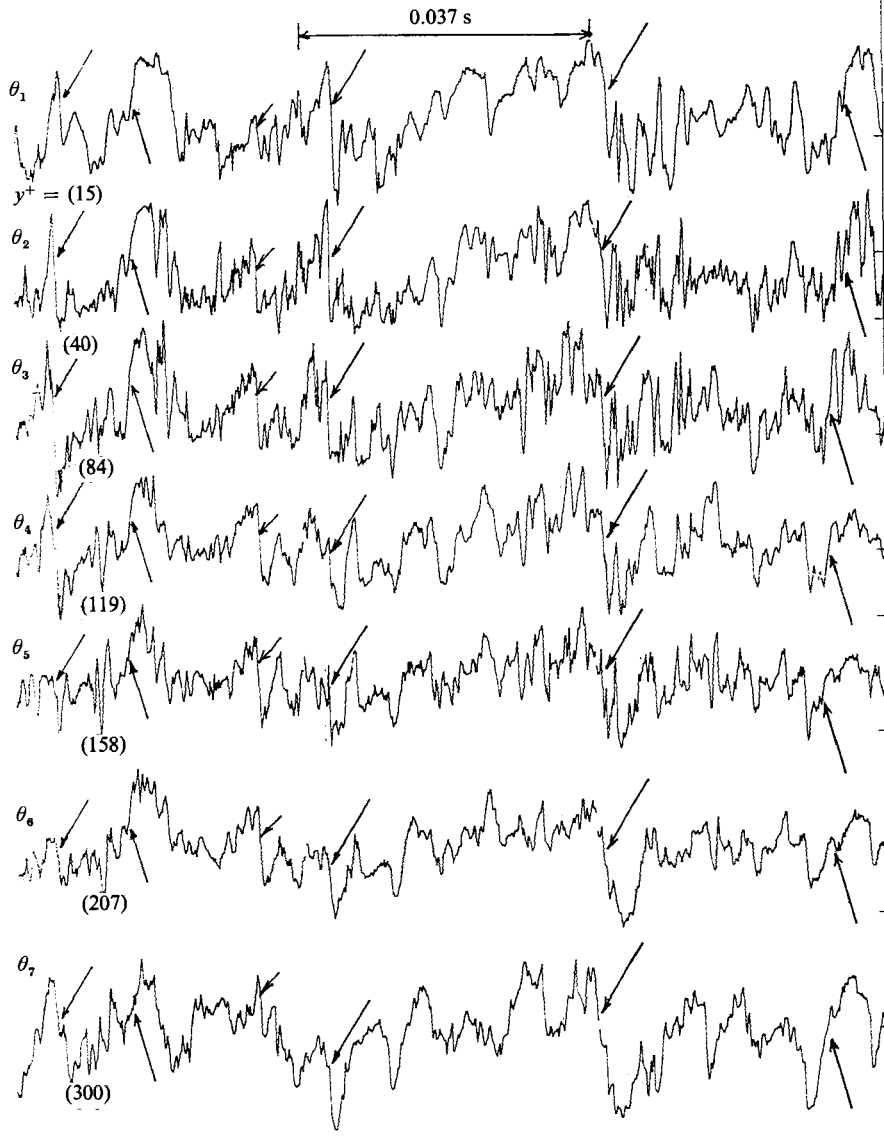
FIGURE 3. Simultaneous temperature signals from an array of cold wires aligned in the y-direction ($A^+ = 0.055$). Coolings and heatings are denoted by downward arrows and upward arrows respectively. Time increases from left to right.

and the sudden outward motion of a low-speed streak (ejection). The quadrant analysis which quantifies these events and was first introduced by Wallace, Eckelmann & Brodkey (1972) classifies all sweeps as flow motions characterized by $u > 0$ and $v < 0$ and all ejections as motions for which $u < 0$ and $v > 0$. Since not all ($u > 0$, $v < 0$) motions are sweeps and not all ($u < 0$, $v > 0$) motions are ejections, we refrain here from using the terms sweep and ejection in connection with heatings and coolings.

In previous investigations (e.g. Chen & Blackwelder 1978; Subramanian & Antonia 1979; Antonia *et al.* 1983) only coolings were considered. Chen & Blackwelder (1978) noted that coolings were important to the flow dynamics since they provided
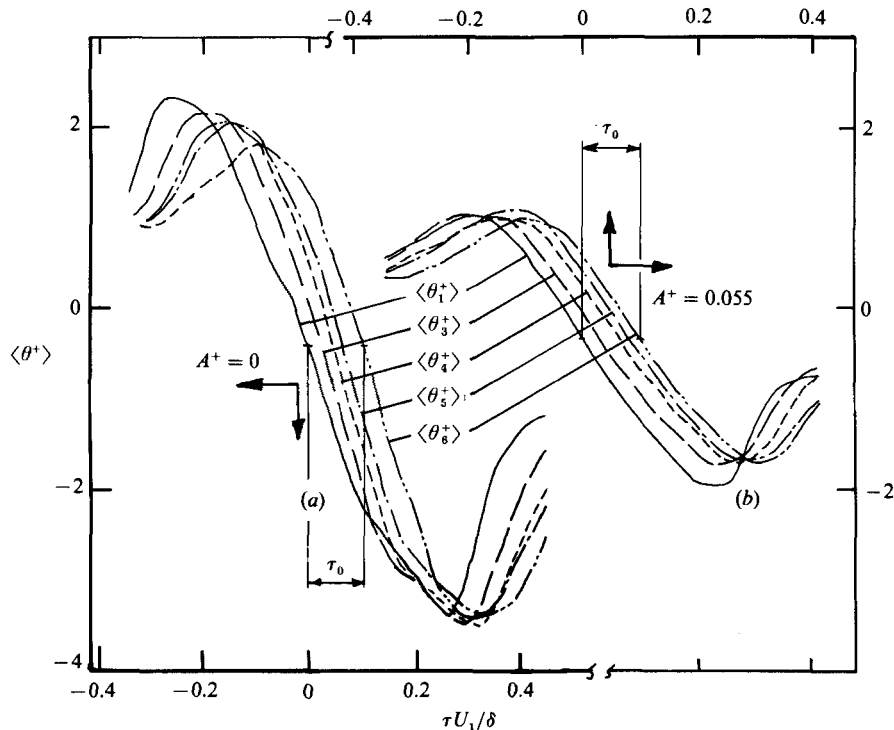
FIGURE 4. Conditional averages of temperature for coolings. Note that the detection is based on
θ_1. (a) $A^+ = 0$, (b) 0.055.

a link between the outer intermittent region and the bursting phenomenon near the wall. These authors assumed that heatings ('warm fronts' in their terminology), because of their lack of spatial coherence, were associated with the random background turbulence. On the basis of the present observations and those of Subramanian et al. (1982), there is no a priori reason for suggesting that heatings are less important, in the context of the flow dynamics, than hot–cold fronts. Both events have therefore been examined here with a view to determining their characteristics. Specifically, we determine their average convection speed in the x-direction by various methods. We also assess the influence of suction on their average shape (in the (x, y)-plane) and their average frequency.

4.1. Convection velocity in the x-direction

Perhaps the simplest way of estimating the average convection speed of the coolings or heatings is by the transit-time method (e.g. Antonia et al. 1979; Subramanian & Antonia 1979): the streamwise separation between any two wires in the array is divided by the average time taken for the coolings or heatings to travel between these two locations. For this purpose, conditional averages of the temperature signals were calculated.

Conditional averages are denoted by angular brackets and are defined by

$$\langle \theta_n(\tau) \rangle = \frac{1}{N} \sum_{i=1}^{N} \theta_n(t_i + \tau),$$
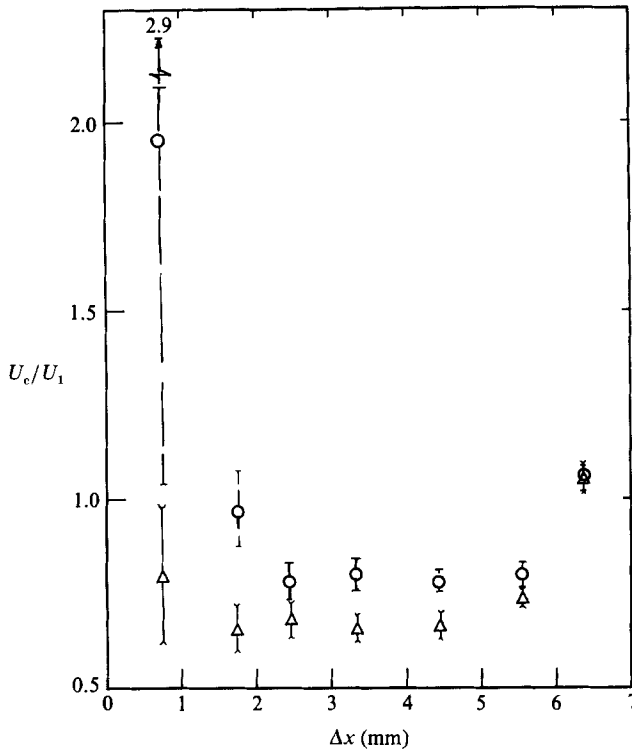
FIGURE 5. Dependence of convection velocity of coolings and heatings on the streamwise separation Δx between cold wires for $A^+ = 0$. ($y^+ \approx 28$ or $y/\delta \approx 0.015$). Vertical bars indicate experimental uncertainties. $\bigcirc$, coolings; $\triangle$, heatings.

where n refers to a particular wire in the array ($n = 1, 2, ..., 8$) and t_i ($i = 1, 2, ..., N$ where N is the total number of detections; typically $N \approx 300$) is the detection instant. The determination of t_i relies on sudden changes (either positive or negative) in the amplitude of all temperature signals in the array being detected within a specified time interval. Detail of the computer algorithm used for this detection are given in the Appendix.

Conditional averages associated with coolings are shown in figure 4 for $A^+ = 0$ and 0.055 but for only five values of n. The peak-to-peak amplitude of $\langle \theta_n \rangle$ tends to decrease as the distance from the detecting location increases. This decrease may be because, although the detection takes into account all temperature signals in the array, conditional averages in figure 4 are calculated using the detection instants appropriate to θ_1. The decrease in the peak-to-peak amplitude of $\langle \theta_n \rangle$ is slower with suction (figure 4b) than without suction (figure 4a) especially when it is realized that the fixed wire spacing of the array implies a larger normalized streamwise distance. Conditional averages, not shown here, for heatings also exhibited the same relative trends as figure 4(a, b). The previous observations tentatively suggest that the streamwise coherence is larger in the case of suction.

The dependence of U_c, approximated by $U_c \approx \Delta x / \tau_0$ (Δx is the distance from the most upstream reference wire and τ_0 is the time interval between the occurrence of an event at any x-location and that at the reference location; the value of τ_0 corresponding to $\langle \theta_6 \rangle$ is shown in figure 4), on the separation Δx is shown in figure 5
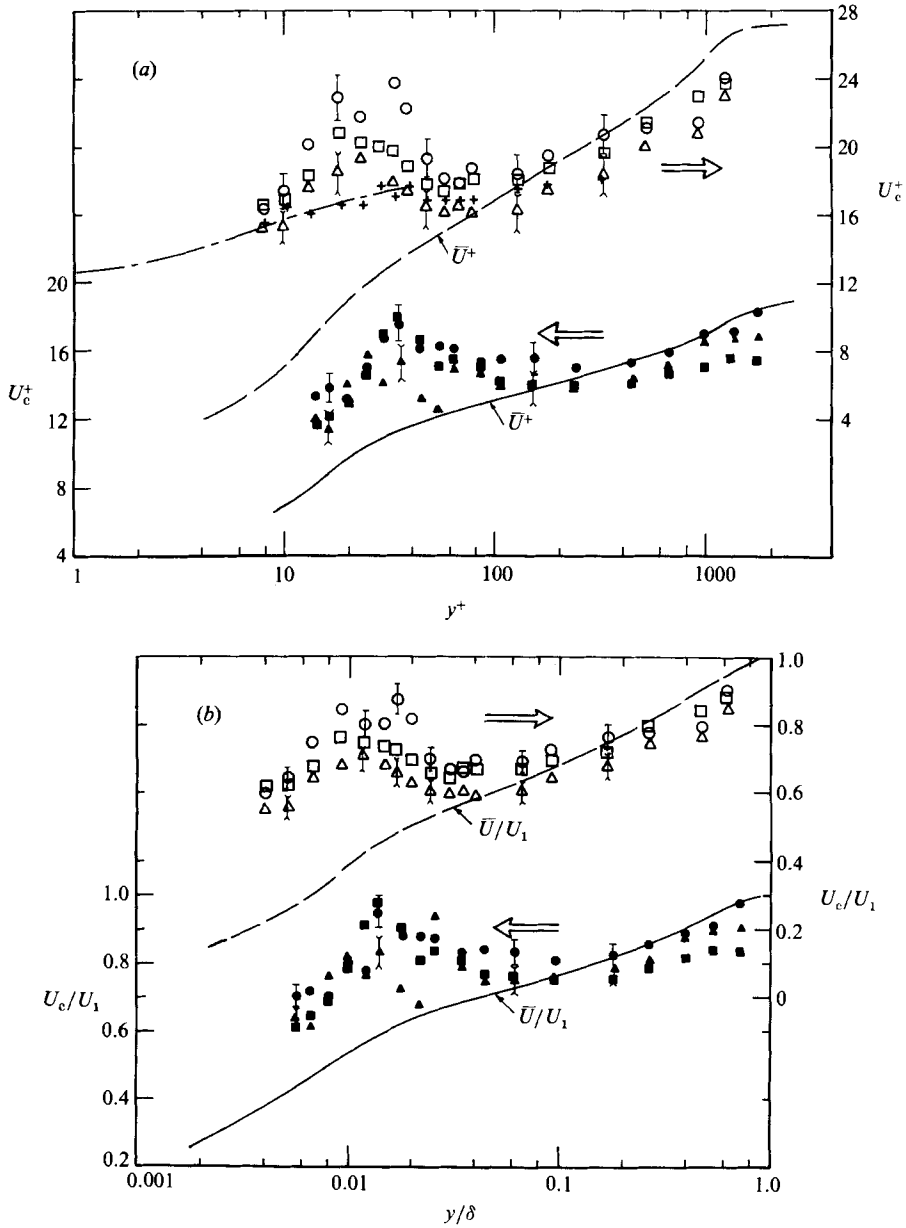
FIGURE 6. Average convection velocity of coolings and heatings, average phase velocity and average convection velocity estimated from conventional space–time correlations. Transit method: ○, coolings; △, heatings. Phase method: □. Space–time correlation method: +, present; —·—, Kreplin & Eckelmann (1979b). Open and closed symbols are for $A^+ = 0$ and $A^+ = 0.055$ respectively. Mean velocity: ——, $A^+ = 0$; ———, $A^+ = 0.055$. (a) U_c^+ vs. y^+; (b) U_c/U_1 vs. y/δ. Vertical bars indicate experimental uncertainties.

for $y^+ = 30$ and $A^+ = 0$. As shown in figure 5, the uncertainty in U_c is largest at small Δx, due to the large uncertainties in Δx and τ_0, and tends to become important at large Δx where the above approximation is inaccurate. However, there is a range of Δx for which U_c is essentially constant ($\pm 5\%$) and it is this value of U_c that has been plotted in figure 6. The results in this figure are for coolings and heatings both

for $A^+ = 0$ and $A^+ = 0.055$. Distributions of the mean velocity $\bar{U}^+$ are also shown in this figure together with estimates of the experimental uncertainties.

As the distance from the wall increases, U_c^+ (figure 6a) first increases, reaching a maximum at $y^+ \approx 20$ for $A^+ = 0$ or $y^+ \approx 30$ for $A^+ = 0.055$, then decreases through the buffer region and the initial part of the logarithmic region. There is a subsequent increase in the outer layer. For heatings, U_c crosses the mean velocity distribution at $y^+ \approx 100$ and remains slightly smaller than $\bar{U}$ throughout the outer layer. For coolings, the crossover point is at a larger distance from the wall. The maximum value of U_c is significant: for $A^+ = 0$, it represents about 80% of the free-stream velocity while for $A^+ = 0.055$, it is almost 90% (figure 6b). Note that the maxima in U_c occur at values of y^+ that correspond approximately to maxima in the production of turbulent energy and temperature variance. The larger convection velocity for coolings than for heatings seems plausible in the sense that the spatial coherence of coolings tends to extend to larger values of y than in the case of heatings. Kline *et al.* (1967) reported measurements of the streamwise velocity of filaments of wall-introduced dye, which move outwards through the boundary layer. The zero-pressure-gradient data indicated that the filament velocity increased between $y^+ \approx 20$ and $y^+ \approx 50$ and gradually decreased at larger y^+. Although the trend of these data is similar to that in figure 6, Kline *et al.*'s filament velocities are consistently smaller than the local mean velocity.

We have included in figure 6(a) the distribution, obtained in an oil duct by Kreplin & Eckelmann (1979b), for the convection velocity of a disturbance 'front' (defined by these authors as a perturbation in velocity that occurs in a space-correlated manner). This convection velocity, inferred from conventional space–time correlations of either u or w, was found to decrease to a limiting value of about $12U_\tau$ at the wall. Although the data of Kreplin & Eckelmann (1979b) are limited, in terms of measurement points and the range of y^+, they suggest a maximum convection velocity of about 85% of the duct centreline velocity. Present near-wall estimates of U_c (figure 6a) inferred from conventional space–time correlations obtained with the x-array data are in good agreement with Kreplin & Eckelmann's (1979b) results. Since conventional space–time correlations give equal weighting to the organized large-scale motion and to the less organized smaller-scale motion, resulting estimates of U_c can differ from convection velocities that relate directly to certain features of the organized motion. In the near-wall region, the convection velocity of coolings is consistently larger than the convection velocity obtained by the conventional space–time correlation method.

U_c was also estimated by the phase method (e.g. Antonia *et al.* 1979, 1983). Briefly, this procedure consists in determining the phase ϕ, defined by $\phi = \tan^{-1}(Q/Co)$, where Q and Co are the quadrature spectrum and cospectrum in the cross-spectrum $G(f)$ between θ_1 and θ_n ($2 \leqslant n \leqslant 8$), viz. $G(f) = Co(f) + iQ(f)$. If it is assumed that turbulence is convected in a frozen pattern, the phase should be given by $\phi = 2\pi f(\Delta x/U_c)$ for small values of the frequency f. The phase *vs.* frequency plot of figure 7 shows a linear relationship at small frequencies, indicating independence of convection velocity of frequency. This relationship is also independent of Δx over the range of Δx used to determine the convection velocity of coolings and heatings. For the range of frequencies used in figure 7, the spectral coherence $Coh(f)$, defined as $Coh(f) = (Co^2 + Q^2)/F_1(f)F_n(f)$ [$F_1(f)$ and $F_n(f)$ are the spectral density functions of θ_1 and θ_n respectively], is in the range 0.7 to 0.98. The convection velocities inferred from the least-square fits† in figure 7 are significnatly larger, both for $A^+ = 0$ and

† The goodness of fit always exceeded 0.99.
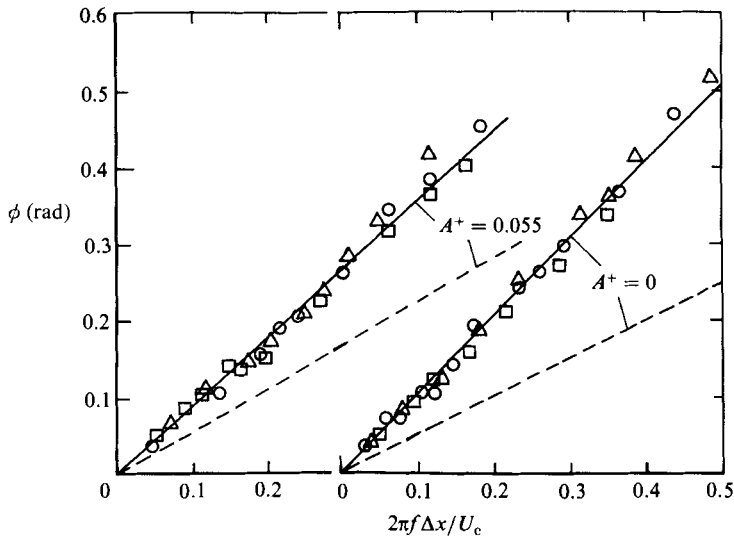
FIGURE 7. Frequency dependence of the phase in the cross-spectrum between θ_1 and any other temperature fluctuation in the x-array of cold wires at $y^+ \approx 20$. $A^+ = 0$: $\bigcirc$, $\Delta x_1 = 3.32$ mm; $\triangle$, 4.44; $\square$, 5.56. $A^+ = 0.055$: $\bigcirc$, $\Delta x_1 = 2.44$ mm; $\triangle$, 3.32; $\square$, 4.44. Solid lines are least-square fits to the data. Broken lines correspond to the local mean velocity.

$A^+ = 0.055$, than the local mean velocities. At this particular location ($y/\delta \approx 0.015$ or $y^+ \approx 28$), U_c/U_1 is 0.8 for a cooling and 0.68 for a heating (see figure 6b). For $A^+ = 0$ ($y/\delta \approx 0.0093$ or $y^+ \approx 19$), U_c/U_1 is 0.76, while for $A^+ = 0.055$ ($y/\delta = 0.008$ or $y^+ = 20$), U_c/U_1 is 0.70. Since the phase method takes into account, at least implicitly, both coolings and heatings, the phase convection velocity is intermediate between the convection velocity of coolings and that of heatings.

4.2. Shape of heatings and coolings

The average position of heatings and coolings in the (x, y)-plane has been estimated using the temperature signals from the y-array and the convection velocity of the events. From distributions of $\langle \theta_n \rangle$ obtained at different y-locations, in similar fashion to those shown in figure 4 at the same y, the time difference τ_1 between the arrival of an event at any y-location and that at the reference location ($y^+ \approx 15$) was estimated. Note that $\tau_1 = 0$ is the detection instant at the reference location. To delineate the average shape of coolings or heatings, τ_1 was converted to a distance Δx_1, relative to the reference location, by multiplying τ_1 by U_c. From the resulting Δy_1^+ vs. Δx_1^+ distributions (figure 8) where Δy_1 is measured from the reference y-value, it can be inferred that the average inclination, $\tan^{-1}(\Delta y_1^+/\Delta x_1^+)$, initially increases away from the reference location and becomes approximately constant for $\Delta y^+ \gtrsim 50$. The increase occurs more rapidly without suction than with suction, especially for coolings. For coolings, the constant inclination ($\approx 40°$), for $\Delta y_1^+ \gtrsim 50$, is essentially unaffected by suction. By contrast, the inclination of heatings, which is approximately 40° without suction, is increased to about 50° for suction. Note that figure 8 shows that there is close agreement between results obtained at different reference locations, reflecting the good internal consistency of the data.

It is of interest to compare the present results for $A^+ = 0$ with results reported in the literature, also for $A^+ = 0$. In a boundary layer, Chen & Blackwelder (1978) reported a value of about 45° for coolings while Head & Bandyopadhyay (1981)
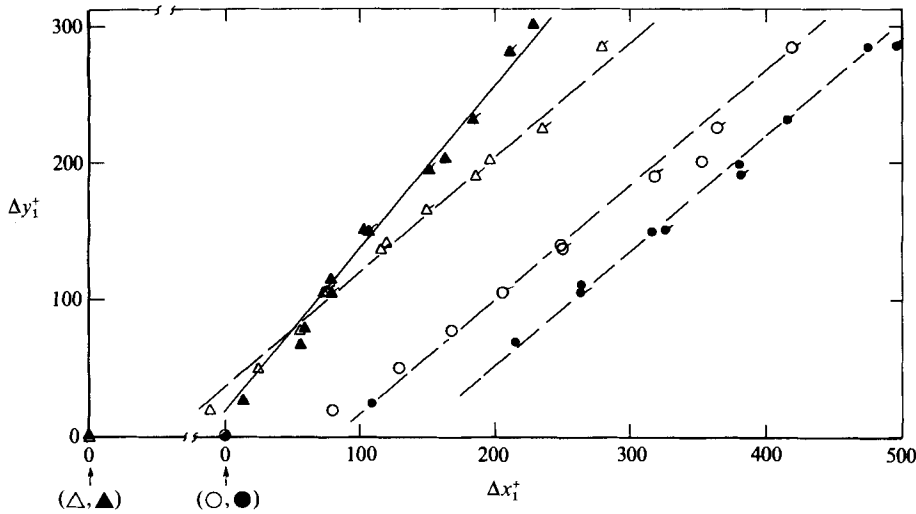
FIGURE 8. Average shape of coolings and heatings in the (x, y)-plane. Δx_1 and Δy_1 are measured with respect to a reference location in the x- and y-directions respectively: $\bigcirc$, coolings; $\triangle$, heatings. Open and closed symbols are for $A^+ = 0$ and $A^+ = 0.055$ respectively. Reference location: $y^+ \approx 15$ (untagged symbols) and $y^+ \approx 110$ (tagged symbols). ——, line of 50° slope; ———, line of 40° slope. Note the shift in origin for the abscissa.

		$\bar{T}U_1/\delta$	
	y^+	Cooling	Heating
$A^+ = 0$	16	8.0	15.0
	70	7.6	19.2
	102	6.9	15.7
$A^+ = 0.055$	15	17.1	40.9
	65	11.3	30.5
	95	8.5	20.3

TABLE 1. Average period of coolings and heatings. y^+ refers to the location, in the y-array, of the wire nearest the wall.

observed that the inclination of elongated vortex loops (or hairpin vortices) was in the range 40–50°. In a turbulent channel flow, Moin & Kim (1985) used a data base generated by a large-eddy simulation technique and found that, away from the wall, the vorticity vector has a maximum inclination of about 45°. The previous observations suggest a close association between coolings or heatings and the vortex loops or hairpin vortices.

4.3. Average frequency of coolings and heatings

The average frequency ($\equiv \bar{T}^{-1}$, where $\bar{T}$ is the mean period) between coolings and heatings was determined by counting the number of events from the temperature signals in the y-array. Initially, events were detected by eye but, since this procedure was tedious, it was replaced by the computer procedure described in the Appendix. Since the aim is to assess the influence of suction on $\bar{T}$ in a qualitative rather than quantitative manner, the use of the algorithm, with the selection parameters kept the same for $A^+ = 0$ and $A^+ = 0.055$, seemed justifiable.

The results are shown in table 1 for three values of y^+. A record duration of 48.4 s was used for $A^+ = 0$ and $A^+ = 0.055$. This duration is larger than the greatest and smallest average periods between events by factors of about 230 and 1400 respectively. Expressed in terms of viscous units, the extent in the y-direction of the array was approximately 200 for $A^+ = 0$ and 300 for $A^+ = 0.055$. For $A^+ = 0$, there are approximately twice as many coolings as heatings, almost independently of y^+. Using VITA, Chen & Blackwelder (1978) found approximately four times as many coolings as heatings. For $A^+ = 0.055$, there is a significant reduction both for coolings and heatings. The increase, due to suction, in $\bar{T}$ is more pronounced for heatings than coolings. Table 1 shows that, as y^+ increases, the effect of suction appears to become less important, $\bar{T}$ approaching the value obtained without suction. This is consistent with Fulachier's (1972) observation that, although suction has an effect on the whole boundary layer, as evidenced for example by the suction-caused decrease in the boundary-layer thickness, the effect is much more pronounced near the wall than in the outer region.

5. Flow visualization results

The flow visualizations reported here focus on two aspects of the organized motion in the layer: the low-speed streaks in the near-wall region and the interaction between the wall region and the outer layer. The manner in which low-speed streaks are influenced by wall suction was inferred from plan views of dye introduced at the wall. Some light was shed on the second aspect by elevation views, or views in the (x, y)-plane, of dye introduced at the wall.

5.1. *Plan views*

Close-up views of the dye near the slit reveal essentially the same features that have been described, using a variety of visualization methods, by others (e.g. Kline & Runstadler 1959; Richardson & Beatty 1959; Kline *et al.* 1967; Smith & Schwartz 1983; Smith & Metzler 1983). Low-speed streaks, visible as regions of accumulation of dye, are formed randomly in space and time although it is evident (this is better seen in the photograph of figure 10 than in figure 9) that small irregularities along the slit act as sites for a high accumulation of dye.

Figure 9 shows that even very small rates of suction ($A^+ = 0.014$) lead to a stabilization of the low-speed streaks. There is a significant reduction in the lateral oscillation of the streaks for $A^+ = 0.014$ compared with $A^+ = 0$. Smith & Metzler (1983) commented, with respect to a boundary layer over an impervious surface, that a unique feature of streaks is their remarkable degree of persistence and regularity (Kline 1978). This feature is further enhanced when suction is applied, the streaks (figure 9) for $A^+ = 0.014$ being longer and more persistent than for $A^+ = 0$. In the latter case, the normalized average length L^+ is about 430 whereas, for $A^+ = 0.014$, we estimate that it is as large as 2300. We also noted that the trend for low-speed streaks to merge or amalgamate when A^+ is zero (e.g. Nakagawa & Nezu 1981; Smith & Metzler 1983) is diminished by suction.

As the suction rate is increased, larger amounts of dye are sucked into the porous plate making visualization quite ambiguous. To assess the influence of suction on the near-wall flow, plan views were taken of the impervious surface downstream of the porous plate (case H2). In figure 10, the effect of suction is seen indirectly since the boundary condition that pertains to the viewed region has changed. The streaks are generally shorter in figure 10(a) for $A^+ = 0$ than in figure 10(b) for $A^+ = 0.047$ (the

(a)   (b)
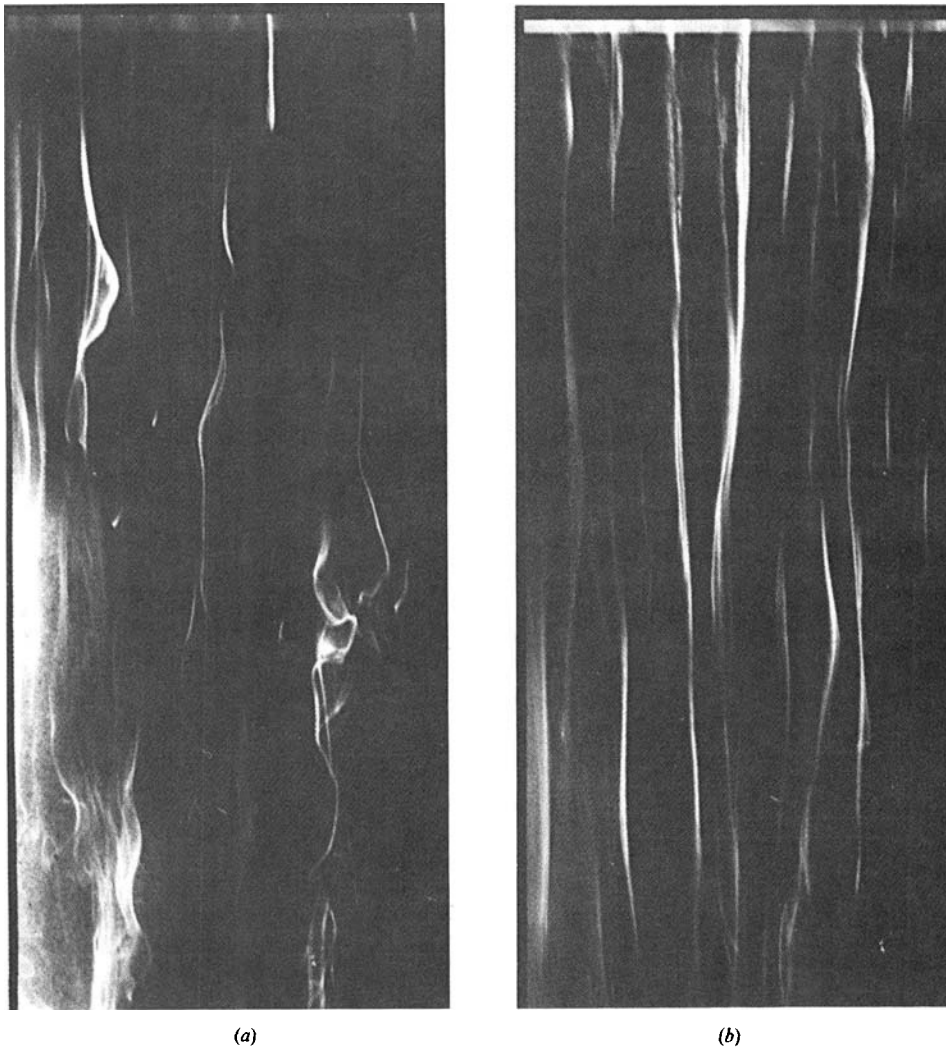
FIGURE 9. Plan view of low-speed streaks for case H1. Flow direction is top to bottom.
(a) $A^+ = 0$, (b) 0.014.

dye flow rate is the same in both cases). The spanwise spacing between streaks is also generally more uniform (as x increases) in figure 10(b) than in figure 10(a). Since the wall flow should respond almost immediately to the new boundary condition, figure 10 implies that there is an important memory effect, i.e. the stabilization of the upstream flow is felt over a significant distance downstream of the porous surface. We also noted, especially from viewing the film for H2, that the stabilization improves as the suction rate is increased.

To estimate λ, the average spanwise separation between low-speed streaks, the latter were counted for case H1 and three values of A^+ (0, 0.014, 0.026). Counting was done at three values of X, the first of these being at $X = 0$ or 30 mm from the slit and the last at $X = 100$ mm where mean velocity profiles were measured. Ten photographs (similar to those in figure 10) were used for each value of A^+ and about 10 streaks were counted on each photograph. The average value of λ^+ as well as its extreme values, corresponding to the smallest and largest numbers of counts, are
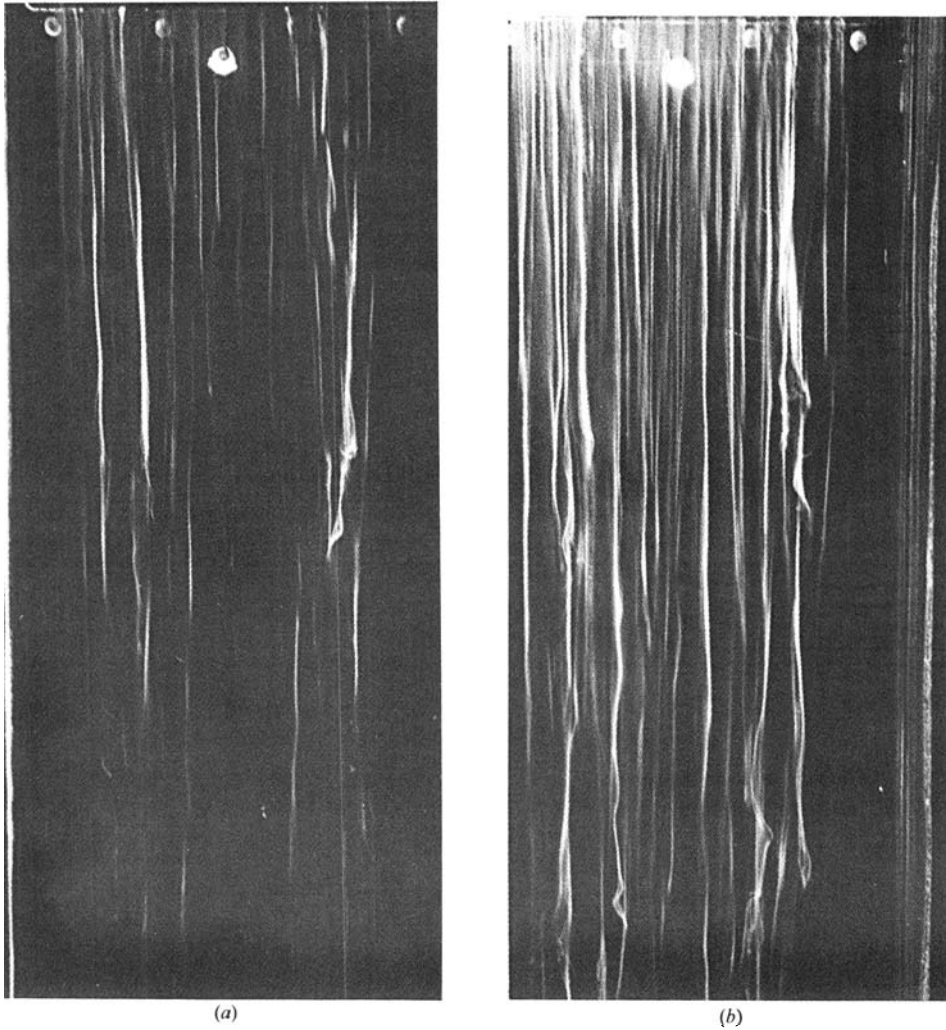
FIGURE 10. Plan view of low-speed streaks for case H2. Flow direction is top to bottom.
(a) $A^+ = 0$, (b) 0.072.

shown in figure 11. The uncertainty is larger for $A^+ = 0$ than with suction since the streaks are more coherent in the latter case. For $A^+ = 0$ and at $X = 100$ mm, λ^+ is about 100, the consensus value obtained in many investigations (e.g. Cantwell 1981). Although the present Reynolds number is small, Smith & Metzler (1983) found that λ^+ is approximately 100 over a relatively wide range of Reynolds numbers. For $A^+ > 0$, λ decreases (e.g. the larger number of streaks in figure 10b than in figure 10a) but, to within the maximum variation of the data (figure 11), there is no significant change in λ^+, the decrease in λ being offset by the increase in the friction velocity. Two reasons may be given for the smaller values of λ^+ at smaller X (figure 11). Near the slit, the low-speed streaks lie closer to the wall than at larger X (from the speed of the dye, we estimated that y^+ was less than unity). Nakagawa & Nezu (1981) and Smith & Metzler (1983) observed that λ increases with y because low-speed streaks are more likely to coalesce than to divide or split. The second, less likely, reason may
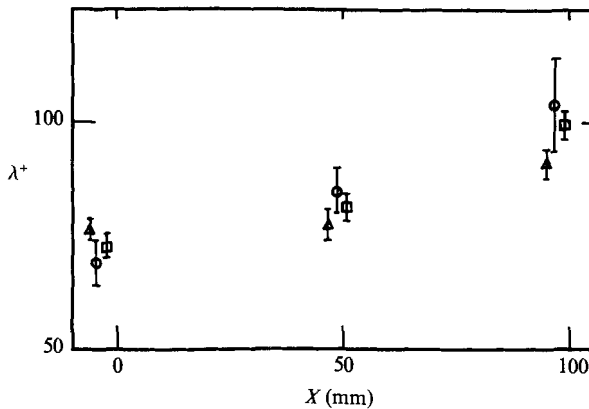
FIGURE 11. Normalized average spanwise spacing of low-speed streaks as a function of distance from the dye slot for case H1. $\bigcirc$, $A^+ = 0$, $\triangle$, 0.014, $\square$, 0.026. (The measurements were made at the same X, but to avoid confusion, the triangles and squares have been displaced slightly.)

be associated with the existence of extremely narrow streaks very close to the wall. This may have been caused by the clinging property of the rhodorsil, perhaps because of its non-Newtonian characteristics. Owing to the small transverse width of these streaks (there is some evidence of this in figure 10 for small X), it was possible to ignore most of them during counting. The possibility that systematic over-counting occurred at small X cannot however be ruled out.

5.2. *Elevation views*

In the absence of suction, photographs and films of the (x, y)-plane indicate that wall-introduced dye often assumes the form of bent-over loops. The latter sometimes stretch out across the external layer while their extremities generally rotate in the same direction as large-scale bulges, suggesting the existence of spanwise vorticity. This observation is very similar to that of Wallace (1985) who noted, for the case of a boundary layer without suction and at a momentum-thickness Reynolds number of 750, that fluid, which is marked with smoke at the wall, can traverse the entire boundary layer. For the photographs of figure 12 (Plate 1), which are for case H1, the upstream boundary layer is coloured with green dye (fluorescein) while white dye is injected at the wall through a hole. The green upstream layer exhibits many of the features observed by Head & Bandyopadhyay (1981) at a comparable Reynolds number. The white loops tend to lift away from the surface, initially at a relatively shallow inclination and subsequently at a much larger inclination, often of the order of 45°. Figure 12 shows that suction reduces the frequency at which the white dye is stretched into the outer layer. This reduction increases as the rate of suction is increased, although an unambiguous interpretation of views (*b*) and (*c*) in figure 12 is difficult because of the partial removal of the dye through the wall. However, we noted, when viewing the film for H2, that there is a decrease in the number of ejections of dye away from the impervious wall as the upstream suction rate is increased. We also observed that dye ejections may be as intense with suction as without it.

The plan and elevation views, obtained with two synchronized cameras, of a single dye filament (figure 13, Plate 1) for case H2 further underline the stabilizing

influence of suction on the near-wall flow. In spite of the imperfections† in the photographs, the latter clearly show a reduction in the amplitude of the spanwise dye excursions as well as an increase in the longitudinal coherence of the dye when suction is applied. The coherence is emphasized by the relatively strong dye concentration for $A^+ = 0.0047$ (figures $13c,d$) compared with $A^+ = 0$ (figures $13a,b$) where the dye trajectory is more diffuse and three-dimensional. There is also evidence in figure $13(c)$ of a relatively violent ejection away from the wall.

6. Concluding discussion

The flow visualizations presented in §5 are fully consistent with the wind-tunnel data described in §§3 and 4 and other previously published measurements. A consistent picture emerges for the effect of suction on the organized motion of the boundary layer; the salient aspects of this picture are discussed below.

Suction causes an appreciable stabilization of the near-wall flow: in particular, the low-speed streaks tend to oscillate less in a spanwise direction while their streamwise persistence is increased. This behaviour is supported by the observed reduction in the r.m.s. spanwise velocity fluctuation and also the decrease in the r.m.s. longitudinal velocity fluctuation. The visualizations by Iritani, Kasagi & Hirata (1985) for the flow over a heated impervious surface indicated a close correspondence between low-speed streaks and high-temperature streaks as well as between high-speed streaks and low-temperature streaks. Since the present visualizations indicate a more orderly behaviour of low-speed and high-speed streaks when suction is applied, one would expect the close similarity between u and θ, observed without suction, to be maintained with suction. This is verified by the present measurements of the r.m.s. longitudinal velocity and temperature fluctuations. It can be inferred from the suction-associated increase in the longitudinal coherence of low-speed and high-speed streaks that integral lengthscales of the turbulence should be larger with suction than without. This is well supported by published integral-lengthscale measurements for both pipe (Eléna 1984) and boundary-layer flows (Fulachier 1972). The stabilization of the near-wall flow due to suction is not unlike the stabilization observed by Kline *et al.* (1967) in the near-wall region of a turbulent boundary layer that is subjected to a favourable pressure gradient. These authors noted that low-speed streaks tended to be longer and more quiescent than with a zero pressure gradient.

Chen & Blackwelder (1978) suggested that coolings provide a dynamical link between the inner and outer regions of the boundary layer. The present elevation views (figure 12) of the dye ejections confirm possibility of direct communication between the wall and the outer region. There are two points of similarity between the dye ejections and the coolings. First, the average shape of the dye ejections is similar to that for coolings. Perhaps more significantly, the average frequency of coolings and dye ejections decreases as the rate of suction increases. This decrease is consistent with the decrease in the average production of turbulent energy and temperature variance that have been obtained (e.g. Fulachier 1972) in the case of suction.

The possibility of a close association between coolings or heatings and the vortex

---

† The spots that appear in the plan views (figure $13b,d$) were caused by bubbles in the black background paper that was glued to the outside wall of the working section for the purpose of taking the photograph. There is also partial reflection of the dye with respect to the wall in the elevation views.
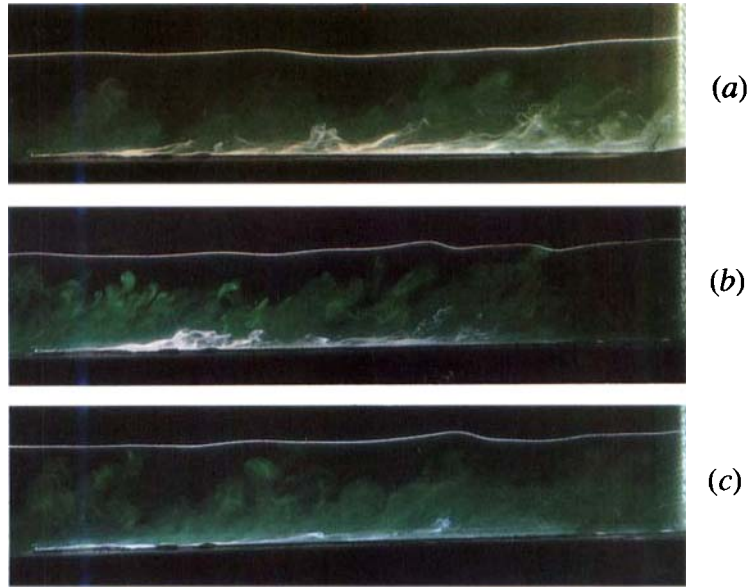
FIGURE 12. Elevation views for case H1 and three values of A^+. White dye is introduced at the wall through a hole 30 mm upstream of $X = 0$. Green dye marks the upstream boundary layer. Flow direction is from left to right. (*a*) $A^+ = 0$; (*b*) 0.047; (*c*) 0.072.

(*a*)   (*b*)   (*c*)   (*d*)
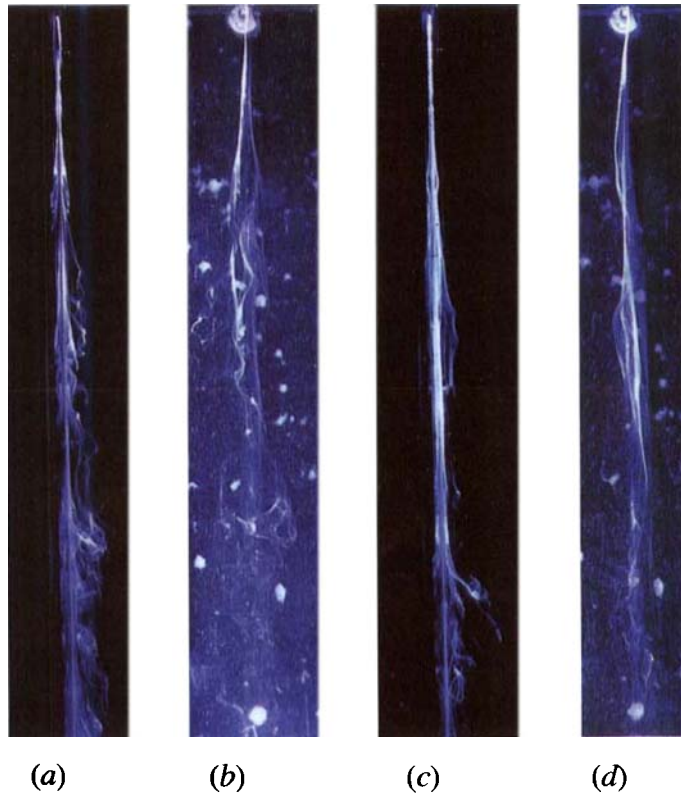
FIGURE 13. Simultaneous plan and elevation views of a single dye filament for case H2. Flow direction is from top to bottom. $A^+ = 0$: (*a*) elevation; (*b*) plan. $A^+ = 0.072$: (*c*) elevation; (*d*) plan.

loops or hairpin vortices (Head & Bandyopadhyay 1981) requires some discussion. As mentioned earlier, it is difficult to draw a direct connection between the dye that is ejected in the (x, y)-plane and the loop vortex. Also, information on the velocity field associated with heatings and coolings is required to confirm the connection between these temperature events and the vortex loops. It is also of interest to investigate the spatial relationship between heatings and coolings; such an investigation is currently being carried out. The fact that the temperature events, like the dye loops, appear to have their origin in the wall region reinforces the importance that has been attached to the vortex loops by, for example, Head & Bandyopadhyay (1981), Wallace (1982) and Smith & Metzler (1983). These last authors emphasized the role that the vortex loops play in the near-wall region in connection with the persistence of the streaks. They suggested that, as these loops move away from the surface, the stretching in the streamwise direction causes the legs of the loops (each leg straddles the streak) to appear as counter-rotating streamwise vortices which act to reinforce the streak.

Near the wall, the average frequency of heatings or coolings is reduced by suction. This result is supported by the reduced number of ejections observed in the flow visualization and leads to the supposition that suction reduces the probability of the breakdown of low-speed streaks. Since this breakdown has been associated with the major source of turbulent-energy and scalar-variance production, this would explain the measured reduction, due to suction, of Reynolds stresses, temperature variances and heat fluxes.

Appendix. Multipoint detection algorithm

The detection procedure is essentially an extension of VITA (Blackwelder & Kaplan 1976) to multipoint data and is similar to a procedure detailed by Bisset, Browne & Antonia (1986).

As noted in the text, coolings and heatings are characterized by sharp changes which occur almost simultaneously in all signals of the array. The reference signal, supplied by the most upstream wire in the x-array or by the wire closest to the wall in the y-array is checked for the following conditions:

$$\psi \equiv \frac{1}{\tau} \int_{-\frac{1}{2}\tau_1}^{+\frac{1}{2}\tau_1} (\theta - \tilde{\theta})^2 \, \mathrm{d}t > k\theta'^2, \tag{A 1}$$

$$\frac{\mathrm{d}\tilde{\theta}}{\mathrm{d}t} < 0 \; (\text{cooling})$$
$$> 0 \; (\text{heating}). \tag{A 2}$$

τ_1 is the moving-window integration time, k the threshold, θ' the conventional r.m.s. of signal and the tilde denotes a mean over the interval τ_1. When (A 1) and (A 2) are satisfied, ψ and $\mathrm{d}\tilde{\theta}/\mathrm{d}t$ are computed over a further interval τ_D, equal to about half the smallest time between successive coolings or heatings. A rough estimate of this latter time is made by inspecting the θ-traces. The instant, which falls inside the interval τ_1, at which ψ is largest and $\mathrm{d}\tilde{\theta}/\mathrm{d}t$ has the correct sign is then taken as a

provisional detection instant. When two provisional detections are found within a time $\frac{1}{3}\tau_D$ of each other (this sometimes occurs because of the superimposed small-scale disturbances) the one with the smaller value of ψ is ignored. Estimates of ψ are then made for each of the other signals of the array over an interval of time, relative to the provisional detection instant, which is large enough to allow the event to be detected by all the wires in the array. Detection instants that satisfy (A 1) and (A 2) are identified for each of these signals. The signals are subsequently time-shifted so that all the detection instants are at the same time location as the reference detection. An average signal θ_{av} is then constructed, viz. $\theta_{av} = B^{-1}(\theta_1 + \theta_2 + \dots + \theta_B)$, where B is the total number of signals, with all the signals centred on the reference detection. The time instants at which the conditions

$$\psi_{av} \equiv \frac{1}{\tau} \int_{-\frac{1}{2}\tau_1}^{+\frac{1}{2}\tau_1} (\theta_{av} - \tilde{\theta}_{av})^2 \, dt > k_{av}\theta'^2 \tag{A 3}$$

and

$$\frac{d\tilde{\theta}_{av}}{dt} < 0 \text{ (cooling)}$$
$$> 0 \text{ (heating)} \tag{A 4}$$

are satisfied are assigned to t_i. Magnitudes of parameters that appear in (A 1)–(A 4) have been optimized by comparing t_i with visually determined detection instants. The same parameters ($k = 1.0$, $k_{av} = 0.7$, $\tau_1 U_1/\delta = 0.6$) were used for $A^+ = 0$ and $A^+ = 0.055$.

REFERENCES

AGGARWAL, J. K., HOLLINGSWORTH, H. A. & MAYHEW, Y. R. 1972 Experimental friction factors for turbulent flow with suction in a porous tube. *Intl J. Heat Mass Transfer* **15**, 1585.

ANTONIA, R. A., BROWNE, L. W. B. & CHAMBERS, A. J. 1981 Determination of time constants of cold wires. *Rev. Sci. Instrum.* **52**, 1382–1385.

ANTONIA, R. A., BROWNE, L. W. B., RAJAGOPALAN, S. & CHAMBERS, A. J. 1983 On the organized motion of a turbulent plane jet. *J. Fluid Mech.* **134**, 49–66.

ANTONIA, R. A., CHAMBERS, A. J., FRIEHE, C. A. & VAN ATTA, C. W. 1979 Temperature ramps in the atmospheric surface layer. *J. Atmos. Sci.* **36**, 101–108.

BISSET, D. K., BROWNE, L. W. B. & ANTONIA, R. A. 1986 Detection of structures in turbulent shear flows. *Rep. T.N. FM* 86/1, Department of Mechanical Engineering, University of Newcastle, NSW.

BLACKWELDER, R. F. & KAPLAN, R. E. 1976 On the wall structure of a turbulent boundary layer. *J. Fluid Mech.* **76**, 89–112.

BROSH, A. & WINOGRAD, Y. 1974 Experimental study of turbulent flow in a tube with wall suction. *Trans. ASME C: J. Heat Transfer* **94**, 338–342.

BRUN, E. A., MARTINOT-LARGARDE, A. & MATHIEU, J. 1970 *Mécanique des Fluides III: Exemples de Phénomènes Instationnaires. Couche Limite et Ecoulements Visqueux.* Paris: Dunod.

CANTWELL, B. J. 1981 Organised motion in turbulent flow. *Ann. Rev. Fluid Mech.* **13**, 457–515.

CHEN, C.-H. P. & BLACKWELDER, R. F. 1978 Large-scale motion in a turbulent boundary layer: a study using temperature contamination. *J. Fluid Mech.* **89**, 1–31.

CLAUSER, F. H. 1956 The turbulent boundary layer. *Adv. Appl. Mech.* **4**, 1–51.

CORINO, E. R. & BRODKEY, R. S. 1969 A visual study of turbulent shear flow. *J. Fluid Mech.* **37**, 1–30.

DUMAS, R., DOMPTAIL, C. & DAIEN, E. 1982 Hydrodynamic visualization of some turbulent flow structures. In *Flow Visualization II* (ed. W. Merzkirch), pp. 393–397. Hemisphere.

ELÉNA, M. 1975 Etude des champs dynamique et thermique d'un ecoulement turbulent en conduite avec aspiration à la paroi. Thèse de Doctorat ès Sciences, IMST, Université d'Aix-Marseille II.

ELÉNA, M. 1984 Suction effects on turbulence statistics in a heated pipe flow. *Phys. Fluids* 27, 861–866.

FAVRE, A., DUMAS, R., VEROLLET, E. & COANTIC, M. 1966 Couche limite turbulente sur paroi poreuse avec aspiration. *J. Méc.* 5, 3–28.

FULACHIER, L. 1972 Contribution à l'étude des analogies des champs dynamique et thermique dans une couche limite turbulente. Effet de l'aspiration. Thèse de Doctorat ès Sciences, Université de Provence.

FULACHIER, L., BENABID, T., ANSELMET, F., ANTONIA, R. A. & KRISHNAMOORTHY, L. V. 1987 Behaviour of coherent structures in a turbulent boundary layer with wall suction. In *Advances in Turbulence* (ed. G. Comte-Bellot & J. Mathieu), pp. 399–407. Springer.

FULACHIER, L., ELÉNA, M., VEROLLET, E. & DUMAS, R. 1982 Suction effects on the structure of the turbulent boundary layer on a heated porous wall. In *Structure of Turbulence in Heat & Mass Transfer* (ed. Z. P. Zaric), pp. 193–220. Hemisphere.

FULACHIER, L., VEROLLET, E. & DEKEYSER, I. 1977 Résultats expérimentaux concernant une couche limite turbulence avec aspiration et chauffage à la paroi. *Intl. J. Heat Mass Transfer* 20, 731–739.

HEAD, M. R. & BANDYOPADHYAY, P. 1981 New aspects of turbulent boundary-layer structure. *J. Fluid Mech.* 107, 297–338.

HISHIDA, M. & NAGANO, Y. 1978 Simultaneous measurements of velocity and temperature in nonisothermal flows. *Trans. J. ASME* C: *J. Heat Transfer* 100, 340–345.

IRITANI, Y., KASAGI, N. & HIRATA, M. 1985 Heat transfer mechanism and associated turbulence structure in the near-wall region of a turbulent boundary layer. In *Turbulent Shear Flows 4* (ed. L. J. S. Bradbury, F. Durst, B. E. Launder, F. W. Schmidt & J. H. Whitelaw), pp. 223–234. Springer.

KAYS, W. M. 1966 *Convective Heat and Mass Transfer*. McGraw-Hill.

KLEBANOFF, P. S. 1955 Characteristics of turbulence in a boundary layer with zero pressure gradient. *NACA Rep.* TN-1247.

KLINE, S. J. 1978 The role of visualization in the study of the structure of the turbulent boundary layer. In *Coherent Structure of Turbulent Boundary Layers* (ed. C. R. Smith & D. E. Abbott), pp. 1–26. AFOSR/Lehigh University Workshop.

KLINE, S. J. & McLINTOCK, F. A. 1953 Describing uncertainties in single-sample experiments. *Mech. Engng* 75, 3–8.

KLINE, S. J., REYNOLDS, W. C., SCHRAUB, F. A. & RUNSTADLER, P. W. 1967 The structure of turbulent boundary layers. *J. Fluid Mech.* 30, 741–773.

KLINE, S. J. & RUNSTADLER, P. W. 1959 Some preliminary results of visual studies of the flow model of the wall layers of the turbulent boundary layer. *Trans. ASME* E: *J. Appl. Mech.* 2, 166–170.

KREPLIN, H.-P. & ECKELMANN, H. 1979a Behaviour of the three fluctuating velocity components in the wall region of a turbulent channel flow. *Phys. Fluids* 22, 1233–1239.

KREPLIN, H.-P. & ECKELMANN, H. 1979b Propagation of perturbations in the viscous sublayer and adjacent wall region. *J. Fluid Mech.* 95, 305–322.

KRISHNAMOORTHY, L. V. & ANTONIA, R. A. 1986 Temperature variance and kinetic energy budgets in the near-wall region of a turbulent boundary layer. In *Proc. 9th Australasian Fluid Mechanics Conference*, pp. 121–124. Auckland.

MOIN, P. & KIM, J. 1985 The structure of the vorticity field in turbulent channel flow. Part 1. Analysis of instantaneous fields and statistical correlations. *J. Fluid Mech.* 155, 441–464.

NAKAGAWA, H. & NEZU, I. 1981 Structure of space–time correlations of bursting phenomena in an open-channel flow. *J. Fluid Mech.* 104, 1–43.

PY, B. 1973 Etude tridimensionnelle de la sous-couche visqueuse dans une veine rectangulaire par des mesures de transfert de matière en paroi. *Intl J. Heat Mass Transfer* 16, 129–144.

RAMNEFORS, M. O. & NYDEN, O. B. 1984 The effect of suction or injection on coherent structures in a turbulent boundary layer. In *Proc. 9th Symposium on Turbulence*, pp. 4–1 to 4–10. University of Missouri-Rolla.

RICHARDSON, F. M. & BEATTY, K. O. 1959 Patterns in turbulent flow in the wall adjacent region. *Phys. Fluids* 2, 718–719.

SCHILDKNECHT, M., MILLER, J. A. & MEIER, G. E. A. 1979 The influence of suction on the structure of turbulence in fully developed pipe flow. *J. Fluid Mech.* **90**, 67–107.

SIRKAR, K. K. & HANRATTY, T. J. 1970 The limiting behaviour of the turbulent transverse velocity component close to a wall. *J. Fluid Mech.* **44**, 605–614.

SMITH, C. R. & METZLER, S. P. 1983 The characteristics of low-speed streaks in the near-wall region of a turbulent boundary layer. *J. Fluid Mech.* **129**, 27–54.

SMITH, C. R. & SCHWARTZ, S. P. 1983 Observation of streamwise rotation in the near-wall region of a turbulent boundary layer. *Phys. Fluids* **26**, 641–652.

SMITS, A. J. & WOOD, D. H. 1985 The response of turbulent boundary layers to sudden perturbations. *Ann. Rev. Fluid Mech.* **17**, 321–358.

STEVENSON, T. N. 1963 A law of the wall for turbulent boundary layers with suction or injection, *Aero Rep.* 166. Cranfield College of Aeronautics.

SUBRAMANIAN, C. S. & ANTONIA, R. A. 1979 Some properties of the large-scale structure in a slightly heated turbulent boundary layer. In *Proc. 2nd Intl Symp. on Turbulent Shear Flow*, pp. 4.18–4.21. London.

SUBRAMANIAN, C. S., RAJAGOPALAN, S., ANTONIA, R. A. & CHAMBERS, A. J. 1982 Comparison of conditional sampling and averaging techniques in a turbulent boundary layer. *J. Fluid Mech.* **123**, 335–362.

TANI, I. 1969 Review of some experimental results on the response of a turbulent boundary layer to sudden perturbations. In *Proc. 1968 AFOSR-IFP-Stanford Conf. on Computation of Turbulent Boundary Layers, Vol. I*, pp. 483–494.

VEROLLET, E. 1972 Etude d'une couche limite turbulente avec aspiration et chauffage à la paroi. Thèse de Doctorat ès Sciences, Université de Provence.

VEROLLET, E., FULACHIER, L. & DEKEYSER, I. 1977 Etude phénoménologique d'une couche limite turbulente avec aspiration et chauffage à la paroi. *Intl J. Heat Mass Transfer* **20**, 107–112.

WALLACE, J. M. 1982 On the structure of bounded turbulent shear flows: a personal view. *Developments in Theoretical and Applied Mechanics*, vol. XI (ed. T. J. Chung & G. R. Karr), pp. 509–521. University of Alabama at Huntsville.

WALLACE, J. M. 1985 The vortical structure of bounded turbulent shear flows. In *Flow of Real Fluid*. Lecture Notes in Physics, vol. 235, (ed. G. E. A. Meier and F. Obermeier), pp. 253–268. Springer.

WALLACE, J. M., ECKELMANN, H. & BRODKEY, R. S. 1972 The wall region in turbulent shear flow. *J. Fluid Mech.* **54**, 39–48.